J Arid Land (2024) 16(3): 373–395
https://doi.org/10.1007/s40333-024-0072-5

Science Press Springer-Verlag

Spatiotemporal variation of land surface temperature and its driving factors in Xinjiang, China

ZHANG Mingyu[1,2], CAO Yu[1,2], ZHANG Zhengyong[1,2*], ZHANG Xueying[3], LIU Lin[1,2], CHEN Hongjin[1,2], GAO Yu[1,2], YU Fengchen[1,2], LIU Xinyi[1,2]

[1] College of Sciences, Shihezi University, Shihezi 832000, China;
[2] Key Laboratory of Oasis Town and Mountain-Basin System Ecology, Xinjiang Production and Construction Corps, Shihezi 832000, China;
[3] Yantai Institute of Coastal Zone Research, Chinese Academy of Sciences, Yantai 264003, China

Abstract: Land surface temperature (LST) directly affects the energy balance of terrestrial surface systems and impacts regional resources, ecosystem evolution, and ecosystem structures. Xinjiang Uygur Autonomous Region is located at the arid Northwest China and is extremely sensitive to climate change. There is an urgent need to understand the distribution patterns of LST in this area and quantitatively measure the nature and intensity of the impacts of the major driving factors from a spatial perspective, as well as elucidate the formation mechanisms. In this study, we used the MOD11C3 LST product developed on the basis of Moderate Resolution Imaging Spectroradiometer (MODIS) to conduct regression analysis and determine the spatiotemporal variation and differentiation pattern of LST in Xinjiang from 2000 to 2020. We analyzed the driving mechanisms of spatial heterogeneity of LST in Xinjiang and the six geomorphic zones (the Altay Mountains, Junggar Basin, Tianshan Mountains, Tarim Basin, Turpan-Hami (Tuha) Basin, and Pakakuna Mountain Group) using geographical detector (Geodetector) and geographically weighted regression (GWR) models. The warming rate of LST in Xinjiang during the study period was 0.24°C/10a, and the spatial distribution pattern of LST had obvious topographic imprints, with 87.20% of the warming zone located in the Gobi desert and areas with frequent human activities, and the cooling zone mainly located in the mountainous areas. The seasonal LST in Xinjiang was at a cooling rate of 0.09°C/10a in autumn, and showed a warming trend in other seasons. Digital elevation model (DEM), latitude, wind speed, precipitation, normalized difference vegetation index (NDVI), and sunshine duration in the single-factor and interactive detections were the key factors driving the LST changes. The direction and intensity of each major driving factor on the spatial variations of LST in the study area were heterogeneous. The negative feedback effect of DEM on the spatial differentiation of LST was the strongest. Lower latitudes, lower vegetation coverage, lower levels of precipitation, and longer sunshine duration increased LST. Unused land was the main heat source landscape, water body was the most important heat sink landscape, grassland and forest land were the land use and land cover (LULC) types with the most prominent heat sink effect, and there were significant differences in different geomorphic zones due to the influences of their vegetation types, climatic conditions, soil types, and human activities. The findings will help to facilitate sustainable climate change management, analyze local climate and environmental patterns, and improve land management strategies in Xinjiang and other arid areas.

*Corresponding author: ZHANG Zhengyong (E-mail: zyz0815@163.com)
The first and second authors contributed equally to this work.
Received 2023-10-20; revised 2024-02-23; accepted 2024-02-26

Keywords: land surface temperature; MOD11C3; climate change; geographical detector (Geodetector); geographically weighted regression (GWR); source-sink effect; Xinjiang

Citation: ZHANG Mingyu, CAO Yu, ZHANG Zhengyong, ZHANG Xueying, LIU Lin, CHEN Hongjin, GAO Yu, YU Fengchen, LIU Xinyi. 2024. Spatiotemporal variation of land surface temperature and its driving factors in Xinjiang, China. Journal of Arid Land, 16(3): 373–395. https://doi.org/10.1007/s40333-024-0072-5

1 Introduction

Land surface temperature (LST) is an essential parameter used to assess the energy exchange between the Earth's surface and atmosphere. It directly affects the energy balance of the Earth's terrestrial surface system and is a visual reflection of regional and global climate change (Tian et al., 2022). As a core element of the climate system, LST is an essential tool for studying and detecting environmental changes (Townshend et al., 1994). The LST evolves from a complex energy transfer and transformation process. Its spatial and temporal differentiation is controlled by many geo-environmental factors influencing the water-heat balance, which in turn affects the resource environment and ecosystem structure (Sfîcă et al., 2023), making it vital for agriculture, hydrology, and ecology (Anderson et al., 2008; Zhang et al., 2009; Li et al., 2013). As a key factor in surface physical processes at global and regional scales, analyzing the spatial and temporal pattern divergence and spatial heterogeneity of LST is essential for analyzing regional climate change processes and driving mechanisms (Xi et al., 2023).

Currently, LST research is widely focused on the urban heat island effect (Ren et al., 2021; Yang et al., 2021; Sfîcă et al., 2023), crop sowing date predictions for agriculture (Zeng et al., 2015; Zhang et al., 2015), drought monitoring (Khan et al., 2018; Hu et al., 2020), soil freeze-thaw analysis (Yue et al., 2021), and human activity intensity research (Portela et al., 2020; Chen et al., 2022a). Although LST is a general term for soil temperature on the surface and at different depths below the ground, there are obvious spatial differences in topography, climatic environment, and underlying surface attributes, which can cause the diversity of LST distribution patterns and the regionality of formation mechanisms (Wu et al., 2022). There are numerous investigations that have analyzed the characteristics of LST changes in China and other regions from the perspectives of temporal and spatial changes, mutation characteristics, influencing factors, and climate change response mechanisms (Huang et al., 2016; Tian et al., 2022; Zhang et al., 2022). There is a consensus that LST will show a significant upward trend in response to climate change (Ren et al., 2021). However, because of the different research areas and periods, the spatial and temporal pattern differentiation and variation ranges are not the same, and the driving mechanisms for the spatial differentiation of LST have not yet been fully elucidated. In particular, the warming and cooling effects of different underlying surfaces and complex geomorphic zones remain unclear. Spatial heterogeneity of LST is also related to the spatial scale; the smaller the scale, the more complex the mechanisms (Ren et al., 2021). At the macro scale, latitude determines the length of solar radiation and the amount of heat, whereas longitude characterizes the location of land and sea and the extent to which the continents influence the formation of the climate of each place (Zhang et al., 2023). Topography is an important parameter for characterizing surface geomorphology at small and medium scales (Tian et al., 2022). It is multifaceted, and the complex geomorphic features of mountains and basins increase its spatial heterogeneity. In addition, owing to the obvious differences in heat budget processes, such as radiation, absorption, reflection, and transpiration, the effects of LST on the underlying surface and feedback mechanisms have significant spatial and temporal differentiation (Wang et al., 2015; Yu et al., 2020; Chi et al., 2021). Various meteorological factors participate in the energy exchange between the land surface and free atmosphere, and different ranges of the thermodynamic cycle in this process also affect the LST (Tian et al., 2022). Previous studies on LST have used the correlation coefficient method to determine the characteristics of the effects of various influencing factors on LST changes (Portela et al., 2020). However, this correlation analysis cannot clarify the contribution of each driving factor to the spatial heterogeneity of LST,

nor can it express the joint control of many factors. When considering the numerous factors that may affect the distribution pattern of LST, a suitable method to quantitatively analyze the spatial heterogeneity of driving factors and the synergy or antagonism between factors is required to reveal the LST differentiation rules and its genetic mechanisms. The geographical detector (Geodetector) model is a new tool for measuring, mining, and analyzing spatial heterogeneity. It can objectively reflect the priority of each driving factor and the joint effect between factors in geographical phenomena (Wang and Xu, 2017). The geographically weighted regression (GWR) model (Brunsdon et al., 1996) can realize local spatial regression modelling of the relationship between independent and dependent variables, revealing the spatial heterogeneity of driving factors. The complementary advantages of the core theories followed by the above models help explore the response mechanisms of the LST distribution in relation to its driving factors from multiple perspectives.

Xinjiang Uygur Autonomous Region in Northwest China is a vast territory that includes oasis, alpine, and dry-hot desert areas (Chen et al., 2022a). It is also an important area of oasis distribution in the arid areas of the world (Pan et al., 2021). As the main gathering place for human activities, oases in arid areas play a decisive role in determining the rationality of agricultural structure, crop growth suitability, and grassland phenology (Zhang et al., 2016; Fu et al., 2017). In addition, as important cold and heat sources, the distribution and development of glacier-frozen soil and the ablation/accumulation of snow cover in alpine frozen and dry-hot desert areas have apparent regulatory effects on the regional energy balance process (Hachem et al., 2012). The stability of desert ecosystems is also affected by the changes in LST (Brenning et al., 2012; Hachem et al., 2012; Zhang et al., 2019). The differences in water, air, and heat conditions of the local underlying surface in the above areas form a significantly different microclimate (Mao et al., 2017), resulting in differences in the heat balance and water volume in the system, which makes the inter-annual and seasonal changes of LST in Xinjiang very different. This study quantitatively characterized the spatial and temporal differentiation of LST in Xinjiang from 2000 to 2020 using the monthly MOD11C3 LST product developed on the basis of Moderate Resolution Imaging Spectroradiometer (MODIS). The dominant driving factors were identified using the Geodetector model, and the spatial heterogeneity of driving factors were analyzed in combination with the GWR model.

The objectives of this study are: (1) to elucidate the inter-annual and seasonal variation characteristics of LST in Xinjiang; (2) to explore the main driving factors affecting the spatial differentiation of LST in Xinjiang; (3) to explore the response patterns of the main driving factors to the spatial heterogeneity of LST in each geomorphic zone of Xinjiang; and (4) to quantitatively analyze the contribution degree of each LULC type to LST in Xinjiang combined with the source-sink theory. This will help explain the evolution of the eco-geographic patterns in the arid regions in a multi-dimensional manner, which can provide scientific reference data to help cope with climate change, harmonize human-land relations, and facilitate regional sustainable development.

2 Materials and methods

2.1 Study area

Xinjiang Uygur Autonomous Region (73°20′–96°25′E, 34°15′–49°10′N; Fig. 1) is located at the northwestern China. Xinjiang is rich in landform types from north to south, including the Altay Mountains, Junggar Basin, Tianshan Mountains, Turpan-Hami (Tuha) Basin, Tarim Basin, Pamir Plateau, Karakoram Mountains, Kunlun Mountains, and Altun Mountains. The Pamir Plateau, Karakoram Mountains, Kunlun Mountains, and Altun Mountains are collectively referred to as the Pakakuna Mountain Group (Ning et al., 2020). The three mountains (the Altay Mountains, Tianshan Mountains, and Pakakuna Mountain Group) and two basins form a closed terrain area. The deep inland position and distance from the ocean make it difficult for ocean airflow to reach the area,

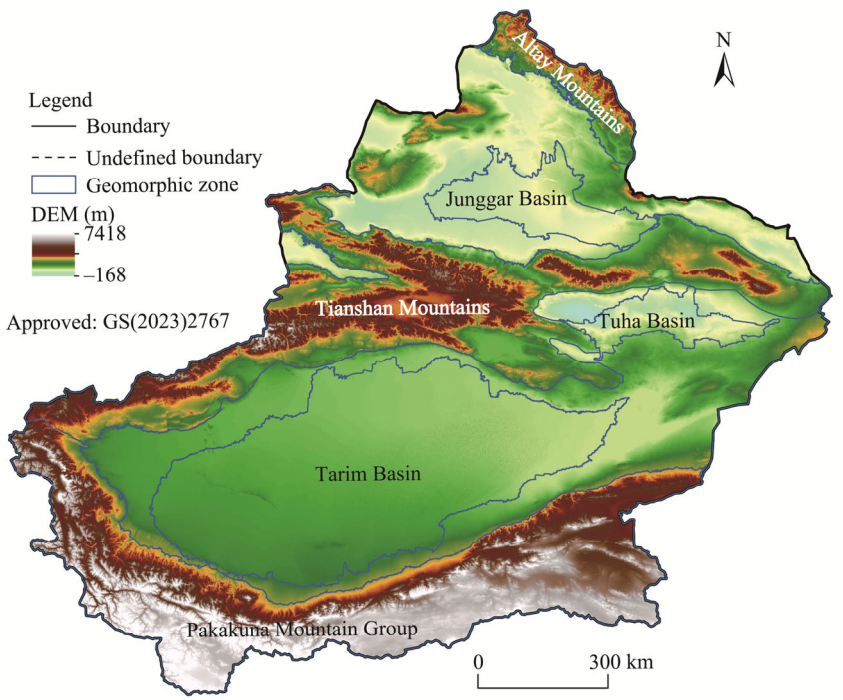

Fig. 1 Overview of Xinjiang Uygur Autonomous Region and the six geomorphic zones (the Altay Mountains, Junggar Basin, Tianshan Mountains, Turpan-Hami (Tuha) Basin, Tarim Basin, and Pakakuna Mountain Group) based on the digital elevation model (DEM). Note that the figure is based on the standard map (GS(2023)2767) of the Map Service System (https://bzdt.ch.mnr.gov.cn/), and the standard map has not been modified. The Pamir Plateau, Karakoram Mountains, Kunlun Mountains, and Altun Mountains are collectively referred to as the Pakakuna Mountain Group.

resulting in a typical temperate continental arid climate with sufficient sunshine, cold winters, and hot summers. The annual average temperature is 6.46℃–9.23℃, and the average annual precipitation is 199.60 mm. Climate differences result in complex oasis-mountain-desert-basin ecosystems, with landform types such as desert, mountain forest, grassland, alpine meadow, and extremely high mountain glaciers (including snow). Although Xinjiang is a vast territory, the land underutilization rate is approximately 61.02%, and consequently, it is susceptible to climate change. The difference in light radiation and energy balance in each landform type causes vertical and horizontal differentiation of LST.

2.2 Data sources

This study used the monthly MODIS-based MOD11C3 LST product data from 2000 to 2020 in Xinjiang to explore the spatiotemporal differentiation characteristics of LST. Precipitation (mm), sunshine duration (h), digital elevation model (DEM; m), normalized difference vegetation index (NDVI), wind speed (m/s), population density (persons/km^2), and land use and land cover (LULC) data were used for the attribution analysis of the spatial heterogeneity in LST (Table 1). We extracted topographic and locational factors such as slope (°), aspect, latitude, and longitude based on DEM data. All data were unified to the WGS-84 coordinate system and UTM projection, and were resampled to 5 km×5 km using the BLINEAR method, except for the LULC.

Two types of MODIS data were used in this investigation. The first type was the MOD11C3 LST product data derived from the MODIS terra global daily surface temperature/emissivity data (https://www.nasa.gov/). The product format was Hierarchical Data File (HDF), and the MODIS Reprojection Tool (MRT) was used for batch processing of mosaicking and reprojection. MOD11C3 contains daytime and nighttime LST data, and an arithmetic average method was

Table 1 Detailed description of data used in the study

Data name	Unit	Period	Resolution	Data source
LST	℃	2000–2020	0.05°	NASA (https://www.nasa.gov/)
NDVI	-	2000–2020	250 m	NASA (https://www.nasa.gov/)
Precipitation	mm	2000–2020	1 km	RESDC (https://www.resdc.cn/)
Wind speed	m/s	2000–2020	1 km	RESDC (https://www.resdc.cn/)
Sunshine duration	h	2000–2020	1 km	RESDC (https://www.resdc.cn/)
Population density	persons/km^2	2020	1 km	WorldPop (https://www.worldpop.org/)
LULC	-	2000, 2010, and 2020	30 m	RESDC (https://www.resdc.cn/)
DEM	m	/	30 m	Geospatial Data Cloud (http://www.gscloud.cn/)
Geomorphic spatial distribution data	-	/	1 km	RESDC (https://www.resdc.cn/)

Note: LST, land surface temperature; NDVI, normalized difference vegetation index; LULC, land use and land cover; DEM, digital elevation model; NASA, National Aeronautics and Space Administration; RESDC, Resource and Environment Science and Data Center. "-" means no unit, and "/" means no data time.

used to obtain seasonal and annual LST. The second type was the MOD13Q1 NDVI data (https://www.nasa.gov/). We synthesized the MOD13Q1 NDVI data with a time resolution of 16 d to monthly NDVI data using the maximum value composite method to reflect the vegetation distribution in different geomorphic zones of Xinjiang on temporal and spatial scales.

The spatially interpolated dataset of average conditions of meteorological elements in China (https://www.resdc.cn/) was based on daily observations of meteorological elements at 2400 stations across the country, with a spatial resolution of 1 km. We selected precipitation, wind speed, sunshine duration data in this study. The population density data were downloaded from WorldPop (https://www.worldpop.org/), which is the current long time-series data with high accuracy and reliability, and has been widely cited for research. The LULC dataset downloaded from the Resource and Environment Science and Data Center (https://www.resdc.cn/) contains data for 2000, 2010, and 2020. Referring to the classification standards of LULC types provided by the Remote Sensing Database of China's Current Land Use Situation combined with the actual situation in the study area, the LULC types were grouped into six categories: forest land, cultivated land, grassland, water body, construction land, and unused land. Based on the DEM data (http://www.gscloud.cn/) and geomorphic spatial distribution data (https://www.resdc.cn/), the actual boundaries of the landforms, such as mountains (groups) and basins, were further revised to provide basic data to explore the spatiotemporal differentiation of LST in various geomorphic zones in Xinjiang.

2.3 Spatiotemporal variation analysis

2.3.1 Trend analysis

The univariate linear regression equation is a reasonably straight line that expresses the relationship between climate and time variables (Zheng et al., 2021). With the help of regression analysis, we conducted a trend analysis of LST at each grid from 2000 to 2020, and the spatial variation characteristics of LST during 2000–2020 were analyzed at annual and seasonal scales. The formula is as follows:

$$\text{Slope} = \frac{\sum_{i=1}^{n} \text{LST}_i i - \frac{1}{n}\left(\sum_{i=1}^{n} \text{LST}_i\right)\left(\sum_{i=1}^{n} i\right)}{\sum_{i=1}^{n} i^2 - \frac{1}{n}\left(\sum_{i=1}^{n} i\right)^2} \times 10, \quad (1)$$

where Slope (℃/10a) is the trend of LST per decade (indicating the rate of change); n is the total number of years; and LST_i (℃) is the land surface temperature in the i^{th} year (i=1, 2, ..., n). When Slope>0, it indicates that the sequence of LST increases with time, and vice versa. The greater the absolute value of Slope, the more pronounced the trend.

2.3.2 Significance test

The significance test describes the possibility of a difference in equation fitting because of sampling error, which can be used to verify and describe the fitting effect of LST and time. The *F*-test evaluates the significance of the rate of change in LST, which represents the credibility of the change trend. The greater the value of *F*, the better the fitting effect and the more pronounced the LST change trend. The formula is as follows:

$$F = U \times \frac{m-2}{Q}, \tag{2}$$

where U is the sum of the squared errors; m is the number of years; and Q is the sum of the regression squares. After reclassifying the significance test results and superimposing the change rate layer, the change trend was divided into six categories as described in Table 2.

Table 2 Classification criteria for the change trend of LST in Xinjiang

Slope	*P*	Change trend
<0	≥0.05	Non-significant deceasing
>0	≥0.05	Non-significant increasing
<0	0.01–0.05	Significant decreasing
>0	0.01–0.05	Significant increasing
<0	<0.01	Highly significant decreasing
>0	<0.01	Highly significant increasing

2.4 Geodetector model

The Geodetector model can detect the driving factors of spatial heterogeneity in the response variables and the influence of the interactions between the driving factors on the response variables. Based on this, we selected 11 driving factors, including longitude, latitude, DEM, slope, aspect, precipitation, sunshine duration, wind speed, NDVI, population density, and LULC, to build an index system, and used the Geodetector model to explore the causes of spatial differentiation in annual LST in Xinjiang. The factor detection model was used to test the explanatory power of each factor on the spatial differentiation patterns of LST, and the interactive detection model was applied to identify the coupling mode between each factor and its influence on the spatial differentiation of LST (Table 3). The formula is as follows:

$$q = 1 - \frac{\sum_{h=1}^{L} N_h \sigma_h^2}{N\sigma^2} = 1 - \frac{SSW}{SST}, \tag{3}$$

where q is the explanatory power of each independent variable on the spatial heterogeneity of LST, and the greater the value, the stronger the explanatory power; L is the stratification of LST (or its driving factors), that is, classification or partitioning; N_h and N are the number of units in the layer h (h=1, 2, ..., L) and the whole region, respectively; σ_h^2 and σ^2 are the variances of LST in layer h and the whole region, respectively; and SSW and SST are the intra-layer variance and total variance of the area, respectively.

The factors affecting LST changes are diverse, and the process mechanisms are complex, including both natural and human factors. Among the natural factors, topography and geographical location factors such as DEM, latitude, longitude, slope, and aspect can affect the balance of solar radiation at different heights and directions. Climatic factors such as wind speed, sunshine duration, and precipitation, can directly affect the total amount of solar radiation received by the surface. NDVI is an essential factor used to characterize surface vegetation coverage, and transpiration of vegetation itself significantly impacts the surrounding environment. Human factors were characterized by population density and LULC in this study, both of which can objectively describe the influence of human activities on surface heat distribution. Population density is mainly characterized by the degree of human aggregation, which transforms the natural environment. Under

Table 3 Description of interaction modes caused by the interaction between driving factors

Description	Interaction mode
$q(X_1 \cap X_2) < \text{Min}[q(X_1), q(X_2)]$	Nonlinear weakening
$\text{Min}[q(X_1), q(X_2)] < q(X_1 \cap X_2) < \text{Max}[q(X_1), q(X_2)]$	Single-factor nonlinear attenuation
$q(X_1 \cap X_2) > \text{Max}[q(X_1), \text{q}(X_2)]$	Two-factor enhancement
$q(X_1 \cap X_2) = q(X_1) + q(X_2)$	Independence
$q(X_1 \cap X_2) > q(X_1) + q(X_2)$	Nonlinear enhancement

Note: X_1 is a driving factor of LST; X_2 is another driving factor of LST; $q(X_1)$ and $q(X_2)$ are the influences of X_1 and X_2 on the spatial heterogeneity of LST, respectively; $q(X_1 \cap X_2)$ is the influence of the interaction of X_1 and X_2 on the spatial heterogeneity of LST. Min, minimum; Max, maximum.

the influence of human activities, changes in LULC types on the surface cause variations in the physical and chemical properties of the underlying surface, thereby enhancing or weakening the reflected solar radiation and affecting the LST distribution.

2.5 GWR model

Traditional global regression assumes that the regression parameters remain unchanged in space, ignoring the spatial heterogeneity between geographical relationships. The GWR model is a spatial regression model based on local smoothness. It obtains local regression coefficients according to different geospatial division units, which can effectively estimate data with spatial autocorrelation and reflect the spatial heterogeneity of driving factors in other regions (Han et al., 2020). This study used the GWR to explore the influence of the main driving factors in each geospatial unit and the differences in the direction and intensity of each action. The formula is as follows:

$$Y_e = \beta_0(u_e, v_e) + \sum_{k=1}^{p} \beta_k(u_e, v_e) x_{ek} + \varepsilon_e, \tag{4}$$

where Y_e is the value of dependent variable at grid e; β_0 is the intercept; (u_e, v_e) is the coordinate of grid e; $\beta_0(u_e, v_e)$ is the constant term of grid e; P is the number of independent variables; $\beta_k(u_e, v_e)$ is the regression coefficient of the k^{th} independent variable (k=1, 2, ..., P) of grid e; x_{ek} is the value of the k^{th} independent variable of grid e; and ε_e is a random error. At the same time, the driving factors were normalized to avoid the influence of outliers and extreme values on the results.

2.6 Source-sink effect on LST

Each LULC type acts as a heat source or sink within a certain area, and the identification of heat source and sink landscape (HSI) can be used to identify the source-sink effect of each LULC type. We calculated the HSI values using the previously reported LST classification with five LST levels: low LST, secondary low LST, medium LST, secondary high LST, and high LST (Wu et al., 2022). Based on the HSI, we calculated the contribution index (CI) to assess the contribution of each heat source or sink landscape to the LST. The formulas are as follows:

$$\text{HSI} = (S_{ahi} / S_a) / (S_{hi} / S), \tag{5}$$

where HSI is the identification of heat source and sink landscapes; S_{ahi} (km^2) is the area of high and secondary high LST zones in LULC type a; S_a (km^2) is the total area of LULC type a; S_{hi} (km^2) is the total area of high and secondary high LST zones in the study area; and S (km^2) is the total study area. When HSI>1.00, the LULC type is defined as the heat source landscape; when HSI<1.00, the LULC type is defined as the heat sink landscape; and when HSI=1.00, the LULC type shows the flow effect.

$$\text{CI} = (T_s - T) \times S_s / S, \tag{6}$$

where T_s (°C) is the average LST of each LULC type in the study area showing sink effect (or source effect); T (°C) is the average LST of the total study area; and S_s (km^2) is the area of each LULC type in the study area showing sink effect (or source effect).

3 Results and discussion

3.1 Spatiotemporal variation characteristics of LST in Xinjiang

3.1.1 Spatiotemporal variation characteristics of annual LST in Xinjiang

The spatial patterns of LST in Xinjiang showed an apparent topographic imprint. The LST was affected by the underlying surface type, topography, and geomorphology, resulting in low values in mountain regions and high values in basin regions (Fig. 2). Overall, the annual average LST of Xinjiang showed a fluctuating upward trend from 2000 to 2020, and varied from 8.53℃ to 10.26℃, with large inter-annual fluctuations and periodic differences (Fig. 3). The multi-year average annual LST in Xinjiang was 9.45℃. The annual average LST in 2007, 2013, and 2015 exceeded 10.00℃ in Xinjiang, with the highest value in 2013 (10.26℃) caused by atmospheric circulation anomalies, which resulted in hot events with broad coverage, high intensity, and long duration (Liu et al., 2021). In addition, the subtropical high in 2013 was significantly stronger than that during the same period, which led to the Tuha Basin as the most significant area affected by high-temperature heat (Dong et al., 2022), where the highest annual average LST was 19.53℃ in 2013. The lowest annual average LST of Xinjiang occurred in 2012 (8.53℃) and this was primarily because of the abnormally cold winter and the long cumulative duration of shallow temperature events in Xinjiang (Chen et al., 2022b).

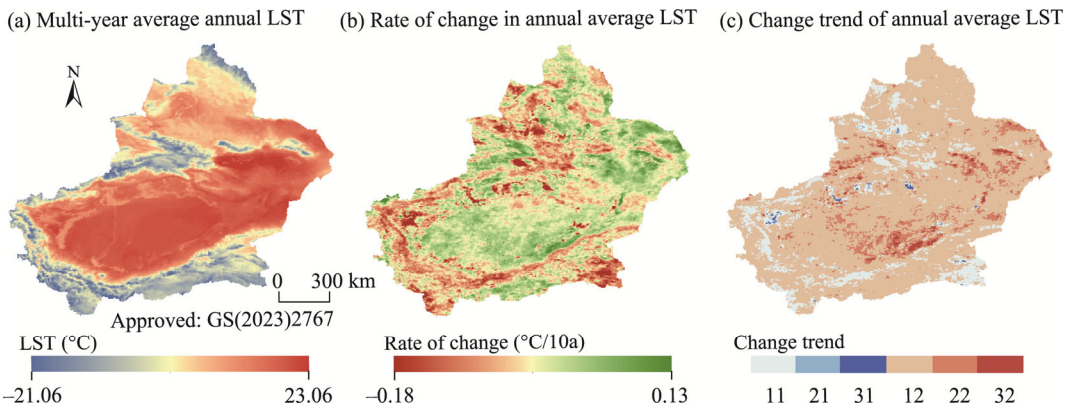

Fig. 2 Spatial distribution of multi-year average annual LST (a), rate of change in annual average LST (b), and change trend of annual average LST (c) in Xinjiang during 2000–2020. LST, land surface temperature. Numbers of 11, 21, and 31 represent non-significant, significant, and highly significant decreasing, respectively; numbers of 12, 22, and 32 represent non-significant, significant, and highly significant increasing, respectively. Note that the figures are based on the standard map (GS(2023)2767) of the Map Service System (https://bzdt.ch.mnr.gov.cn/), and the standard map has not been modified.

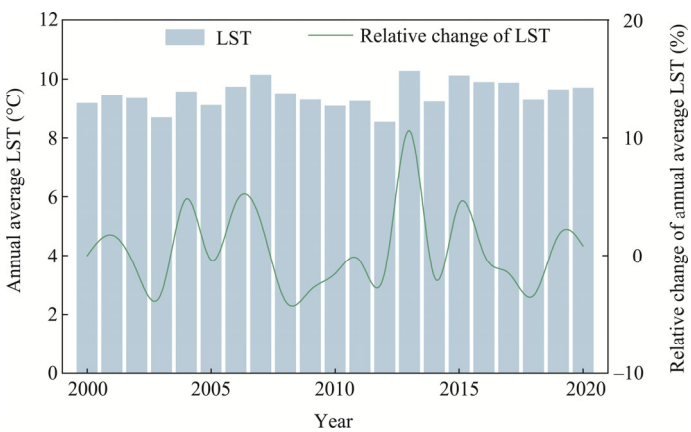

Fig. 3 Temporal variation of annual average LST in Xinjiang from 2000 to 2020

The rate of change for annual LST in Xinjiang was 0.24℃/10a. It showed an annular desuperheating zone surrounded by plains and mountains (Fig. 2b). The warming trend (0.24℃/10a) was not only higher than that of the global LST (0.18℃/10 a; Li et al., 2020) but also higher than that in China (0.21℃/10a; Tian et al., 2022). In addition, the LST in Xinjiang was primarily characterized by non-significant increasing during 2000–2020 (Fig. 2c). The areas that passed the F test (P<0.05) only accounted for 10.36% of the total area, whereas the significant warming area accounted for 8.57% and the highly significant warming area occupied 1.27%. These areas were primarily in the southwest of the Tarim Basin, Tuha Basin, Ili River Valley (western Tianshan Mountains), and Harketawu Mountains (southwestern Tianshan Mountains).

3.1.2 Spatiotemporal differentiation characteristics of annual LST in geomorphic zones

Spatially, the highest multi-year average annual LST in the geomorphologic zones was 23.06°C (Fig. 2a). The Tuha Basin, which is in the middle latitude, had the highest annual average LST (regional average of 20.06°C) in 2017, followed by the Tarim Basin (regional average of 18.03°C) in 2013, and the high-value areas were predominantly beside deserts. Low-value areas were primarily located in the three mountain systems. Although the latitude of the Pakakuna Mountain Group is low, the lowest multi-year average annual LST was –21.06℃ due to its high DEM. The Tianshan Mountains have abundant underlying surfaces, including the Gobi desert, forest lands, and grasslands. The lowest multi-year average annual LST of the Tianshan Mountains was –21.92℃ and the highest value (19.05℃) was adjacent to the Tarim Basin. Although the latitude of the Tianshan Mountains is higher than that of the Pakakuna Mountain Group, their multi-year average annual LST was higher (regional average of 5.77°C). The Altay Mountains have the highest latitude, and their multi-year average annual LST was –1.35℃, the lowest LST among the six geomorphic zones (Fig. 4).

Among the six geomorphological zones (Table 4), the rate of change for annual LST in the Tuha Basin was 0.44℃/10a, which was the fastest warming area in Xinjiang, followed by the Tarim Basin (0.32℃/10a), whereas the LST increase rate for the Pakakuna Mountain Group was the smallest (0.13℃/10a). In Xinjiang, 87.20% of the warming area was concentrated in the Gobi Desert and areas with frequent human activities. The warming rate in some areas of the Tuha Basin can reach 0.96℃/10a. The cooling areas were primarily located in the pre-mountain basins and oasis plain areas with high vegetation coverage. The Pakakuna Mountain Group was the dominant cooling area,

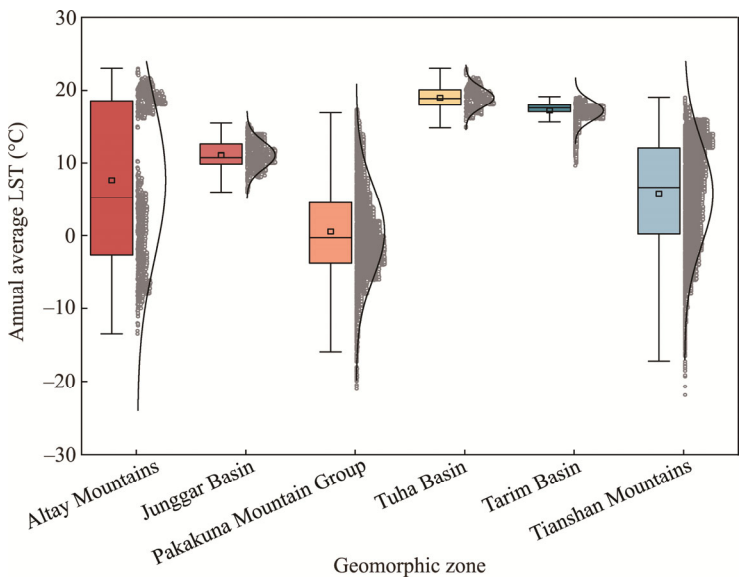

Fig. 4 Distribution characteristics of multi-year average annual LST in various geomorphic zones in Xinjiang. The upper and lower horizontal lines represent the maximum LST and minimum LST, respectively; the bottom and top lines of the box represent the 25th and 75th percentile quartiles, respectively; the line and square in the middle of the box represent the average and median of LST, respectively; and the right-hand dots and trend lines represent the data points and the distributions, respectively.

Table 4 Statistical results of the multi-year average annual LST and rate of change of annual LST, as well as the area proportions of warming area and cooling area in Xinjiang and each geomorphic zone during 2000–2020

Geomorphic zone	Multi-year average annual LST (℃)	Rate of change of annual LST (℃/10a)	Proportion of warming area (%)	Proportion of cooling area (%)
Xinjiang	9.45	0.24	87.20	12.80
Tarim Basin	17.17	0.32	95.90	4.10
Pakakuna Mountain Group	0.54	0.13	73.18	26.82
Tuha Basin	19.02	0.44	99.93	0.07
Altay Mountains	–1.35	0.27	97.19	2.81
Tianshan Mountains	5.77	0.22	85.16	14.84
Junggar Basin	11.06	0.30	93.72	6.28

Note: Tuha, Turpan-Hami. The Pakakuna Mountain Group includes the Pamir Plateau, Karakoram Mountains, Kunlun Mountains, and Altun Mountains.

with the fast cooling rate of –1.55°C/10a in some areas; the Tianshan Mountains had the fast cooling rate of –0.94°C/10a in some areas, and the Yulduz Basin (Central Tianshan Mountains) in the central part and the Bogda Mountains (eastern Tianshan Mountains). The warming area for each geomorphic zone was greater than the cooling area. The cooling area in the Pakakuna Mountain Group (with area proportion of 26.82%) and the Tianshan Mountains (14.84%) accounted for a large proportion of their respective total area. The proportions of warming area in the Tuha Basin and Altay Mountains were more than 97.19%. After testing the significance of the LST change rate in each geomorphic zone, 39.36% of the Tuha Basin was significant ($0.01 \leq P < 0.05$) and 4.04% was highly significant ($P < 0.01$) in warming or cooling. Only 0.11% of the Altay Mountains were significant ($0.01 \leq P < 0.05$) in warming or cooling.

In summary, the LST in Xinjiang showed a warming trend with a high level of heating intensity over a wide area. The warming trend in the basin regions was more significant than that in the mountainous regions. The Tuha Basin and Tarim Basin were the most stable geomorphic zones for warming. The cooling trend mainly appeared in mountainous areas; however, many significant warming areas were located west of the Tianshan Mountains.

To further explore the variation characteristics of LST at different latitudes and longitudes in Xinjiang, we selected 87.30°E (through the Pakakuna Mountain Group, Tarim Basin, Tianshan Mountains, Junggar Basin, and Altay Mountains) and 43.30°N (through the Ili River Valley, Tianshan Mountains, Bogda Mountains, and Barkol Mountains (eastern Tianshan Mountains)) to analyze the latitudinal and longitudinal differentiation of LST (Fig. 5). Lines of longitude (87.30°E) and latitude (43.30°N) cross the main geomorphic zones and can be used to reflect the variation characteristics of LST in different geomorphic zones.

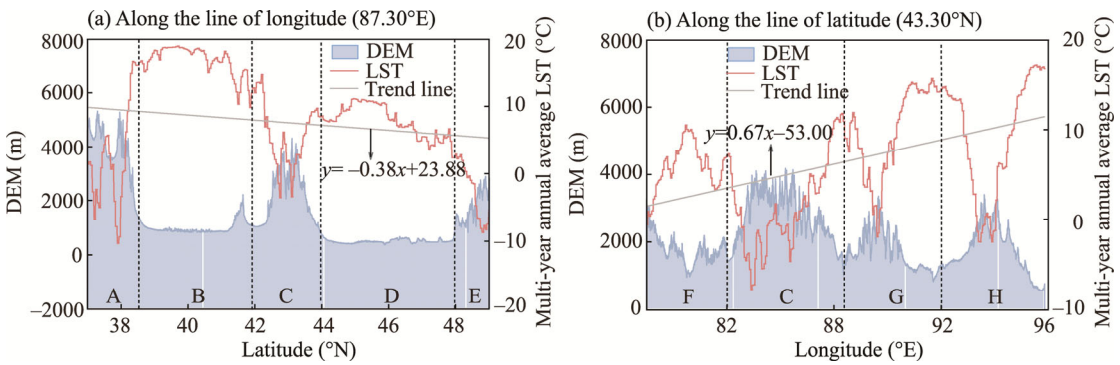

Fig. 5 Variations in the multi-year average annual LST and DEM along (a) the line of longitude (87.30°E) and (b) the line of latitude (43.30°N). A–H represent the Pakakuna Mountain Group, Tarim Basin, Tianshan Mountains, Junggar Basin, Altay Mountains, Ili River Valley, Bogda Mountains, and Barkol Mountains, respectively.

The distribution of LST followed a latitudinal zonal law (Fig. 5a). For every degree of latitudinal increase from south to north, the LST decreased by 0.38℃. However, DEM significantly weakened the latitudinal zonal characteristics of LST in each geomorphic zone. From south to north, the average LST of the Pakakuna Mountain Group passing by the line of longitude (87.30°E) (Fig. 5a) was –1.25℃, the average LST of the Tianshan Mountains reached 7.75℃, and that of the Altay Mountains decreased to –3.00℃; the high values were distributed in the two basins, and the LST in the Junggar Basin was lower than that in the Tarim Basin (which is at a lower latitude). Although the latitude of the Tianshan Mountains is higher than that of the Pakakuna Mountain Group, the LST was higher at some regions, which may be due to the significant warming effect of the Tianshan Mountains (Zhang et al., 2023). The LST decline rate on the southern slope of the Tianshan Mountains was lower than that on the northern slope, primarily because it was sunny, at a lower latitude, and had a lower vegetation coverage. The LST significantly increased from west to east (Fig. 5b); for every degree of longitudinal increase, the LST increased by 0.67℃. The LST in the middle of the Ili River Valley reached approximately 10.53℃ whereas in the middle of the Tianshan Mountains, the lowest LST was –3.47℃; in the Bogda Mountains and Barkol Mountains, the lowest LST was –2.49℃, because of the influence of the surrounding Gobi Desert and vegetation coverage. The LST in the lower DEM of the Bogda Mountains and Barkol Mountains can be as high as 17.25℃, whereas in the middle of the Tianshan Mountains, it was significantly lower than that of the Bogda and Barkol mountainous areas at the same latitude.

The LST gradually decreased from the bottom of the valleys to the top of the mountains, and the spatial variation of certain terrains and underlying surface properties also reduced the latitudinal zonality of the ground temperature. Further exploration of the correlation between LST and DEM revealed that the law of vertical decline of LST restricted its distribution (Table 5). The correlation between LST and DEM in Xinjiang was stronger than that in the first step of geomorphic partitioning in China (Tian et al., 2022). The negative correlation between LST and DEM in the Pakakuna Mountain Group was the strongest, with a correlation coefficient reaching –0.91, followed by the Altay Mountains (–0.87). The vertical decline rates of LST in each mountainous zone are shown in Table 5. Although the Altay Mountains in the northernmost part of the study area have lower DEM and high in latitude, they have large differences in their ability to obtain solar radiation, thus they have the largest vertical decline rate of LST, and the LST is most significantly affected by elevation. Although the Pakakun Mountain Group has a high absolute elevation and a large degree of undulation, the lower latitude makes it obtaining abundant solar radiation, thus weakening the vertical dependence of LST. It can be seen that the latitudinal and altitudinal dependence of LST was more significant in each geomorphic zone. The LST distribution associated with solar radiation had latitudinal zonal characteristics. However, DEM and subsurface characteristics can strengthen the spatial heterogeneity of LST because they can affect local surface thermal properties, resulting in spatial differentiation patterns at the same latitude with lower or higher temperatures.

Table 5 Correlation coefficients between LST and DEM in Xinjiang and three mountainous regions

Geomorphic zone	Correlation coefficient	Vertical decline rate of LST (℃/100 m)
Xinjiang	–0.80	0.45
Altay Mountains	–0.87	0.72
Tianshan Mountains	–0.86	0.66
Pakakuna Mountain Group	–0.91	0.54

3.2 Spatiotemporal variations of seasonal LST in Xinjiang

Seasonal variations of LST in Xinjiang have led to significant differences in vegetation phenology, snow freezing and thawing, and glacier ablation (Shi et al., 1991); thus, this analysis is crucial for the regulation of ecosystem and water resource. The multi-year average LST of Xinjiang in spring and autumn was 11.97℃ and 9.34℃, respectively. The spatial distribution pattern of LST in spring and

autumn was similar (Fig. 6). The low-temperature area (below zero) was in the alpine regions with an average DEM higher than 4329 m in the three mountain systems. The multi-year average LST of Xinjiang in summer was 24.95℃, and the low-temperature areas were only located in the Pakakuna Mountain Group and Hantengri Peak (in the Tianshan Mountains). In winter, the multi-year average LST of Xinjiang was –9.04℃, with higher values in the south and lower values in the north when bounded by the Tianshan Mountains. Only a small area of high LST was found in the southern hinterland of the Tarim Basin.

Of the LST changes across the four seasons in Xinjiang, only autumn experienced a cooling rate of 0.09℃/10a, and the rest of the seasons showed a warming trend, with the largest rate of change in spring (0.49℃/10a), followed by winter (0.48℃/10a) (Table 6). In spring, the warming area in Xinjiang (accounting for 88.74% of the total area) was 7.8 times larger than that of the cooling area. The Tianshan Mountains and Pakakuna Mountain Group were the geomorphological zones with the slowest rate of warming and the largest cooling area, whereas the rate of warming in the Altay Mountains and Junggar Basin was greater than 0.85℃/10a. The warming trend in the Altay Mountains, the eastern part of the Tianshan Mountains, and the southern part of Xinjiang showed a high level of significance.

In summer, the warming area in Xinjiang decreased to 83.32% of the total area, of which 67.41% showed significant warming and the fastest warming rate was 0.64℃/10a in the Tarim Basin; a highly significant cooling zone appeared in the economic zone on the northern slopes of the Tianshan Mountains and along the Tarim Basin, which are areas with rapid economic development in Xinjiang. The significant increase in vegetation coverage because of the artificial intervention reduced surface albedo, increased soil moisture, and produced an important cold zone, which also confirmed that the transformation of the LULC types and physical properties caused by changes in vegetation coverage and human activities were closely linked to changes in the LST (Huang et al., 2016).

The warming area was reduced to minimum in autumn, with 60.87% of the area in Xinjiang showing cooling, and most of the regions showed non-significant warming or cooling. The Altay Mountains had the fastest cooling rate (–0.42℃/10a), and only the Tuha Basin and Pakakuna Mountain Group were in a warming situation at this time. The warming area in winter increased to 84.16% of the area in Xinjiang, and most of the cooling areas were in the Tianshan Mountains and Pakakuna Mountain Group, which were still dominated by insignificant warming or cooling. At this time, the warming rate of the Altay Mountains increased to 0.88℃/10a, followed by that of the Junggar Basin and Tarim Basin. Overall, LST changes in most parts of Xinjiang fluctuated sharply with the seasons, and all the geomorphic zones, except for the Pakakuna Mountain Group, followed the change rate of seasonal LST for the entire Xinjiang, which to a certain extent reflects its climatic sensitivity and indicative nature.

3.3 Dominant factors driving the spatial heterogeneity of LST

3.3.1 Dominant factor identification using the Geodetector model

Previous studies have indicated that there are spatial differences in the LST changes in Xinjiang (Kang et al., 2022). To this end, possible driving factors related to LST changes were identified. All 11 selected factors passed the confidence test and had significant relationships with the LST distribution pattern in Xinjiang. The factor detection results showed that topographic factors had the highest contribution to the spatial differentiation of LST in Xinjiang, followed by natural factors (Fig. 7a). Among them, DEM, wind speed, and latitude had the most prominent explanatory power, with q values of 0.698, 0.503, and 0.392, respectively. In general, the higher the DEM, the thinner the air, and the long-wave radiation received by the ground indirectly restricts vertical heat transfer through the conversion of surface latent heat and heat energy (Wan et al., 2012). Wind speed indirectly affects changes in LST through the dynamic effects of surface heat (Zhou et al., 2014). Excessive wind speeds generated at higher LST will result in air absorbing and removing heat from the surface more rapidly. The faster the air that absorbs and removes surface heat (Garratt, 1994),

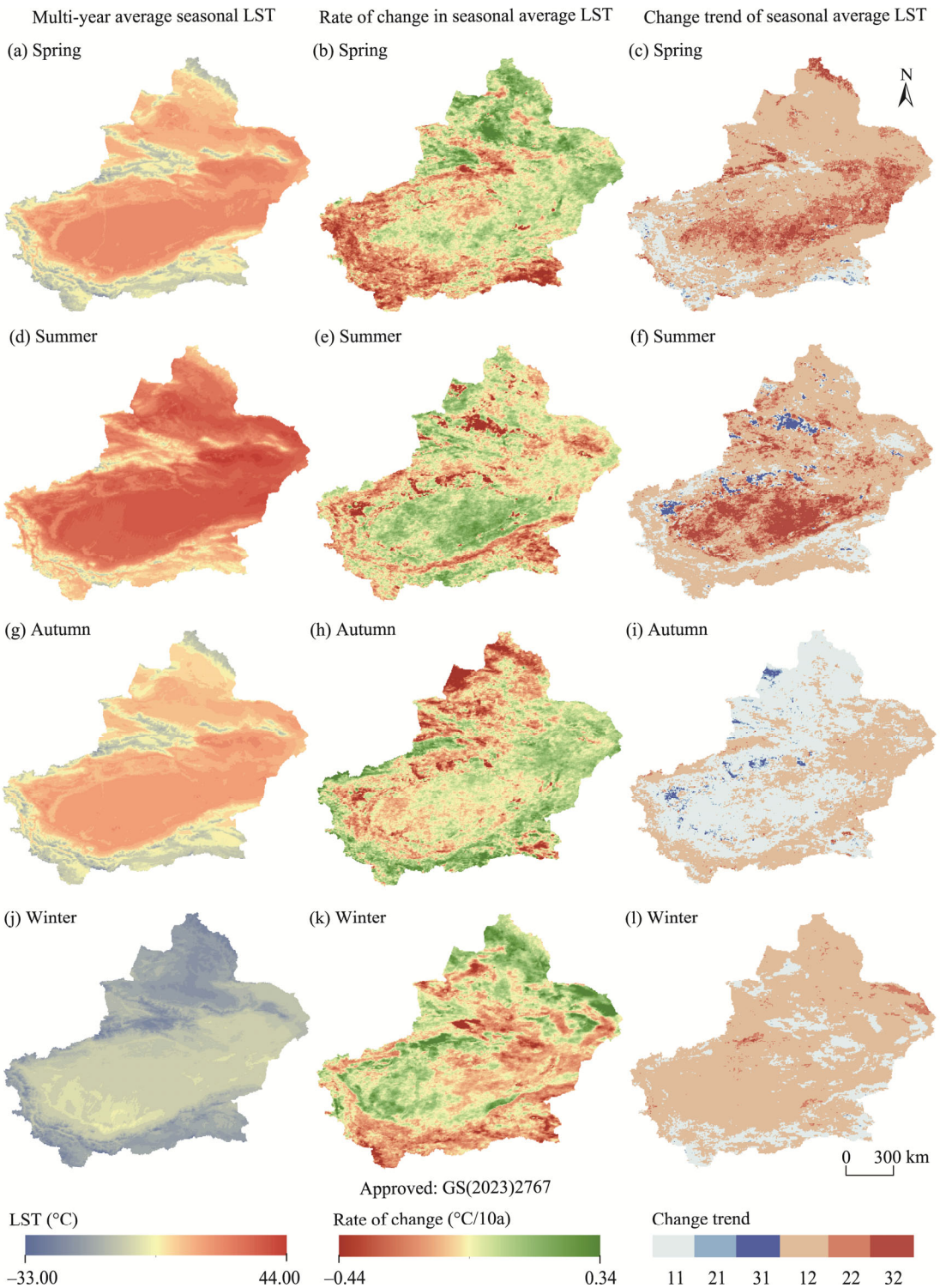

Fig. 6 Spatial distribution of multi-year average seasonal LST (a, d, g, and j), rate of change in seasonal average LST (b, e, h, and k), and change trend of seasonal average LST (c, f, i, and l) in Xinjiang during 2000–2020. Numbers of 11, 21, and 31 represent non-significant, significant, and highly significant decreasing, respectively; numbers of 12, 22, and 32 represent non-significant, significant, and highly significant increasing, respectively. Note that the figures are based on the standard map (GS(2023)2767) of the Map Service System (https://bzdt.ch.mnr.gov.cn/), and the standard map has not been modified.

Table 6 Rate of change in seasonal LST in Xinjiang and each geomorphic zone during 2000–2020

Geomorphic zone	Rate of change in seasonal LST (℃/10a)			
	Spring	Summer	Autumn	Winter
Xinjiang	0.49	0.34	–0.09	0.48
Altay Mountains	0.88	0.32	–0.42	0.88
Junggar Basin	0.85	0.32	–0.16	0.71
Tianshan Mountains	0.48	0.30	–0.05	0.45
Tuha Basin	0.67	0.38	0.14	0.44
Tarim Basin	0.49	0.64	–0.11	0.53
Pakakuna Mountain Group	0.14	0.18	0.07	0.11

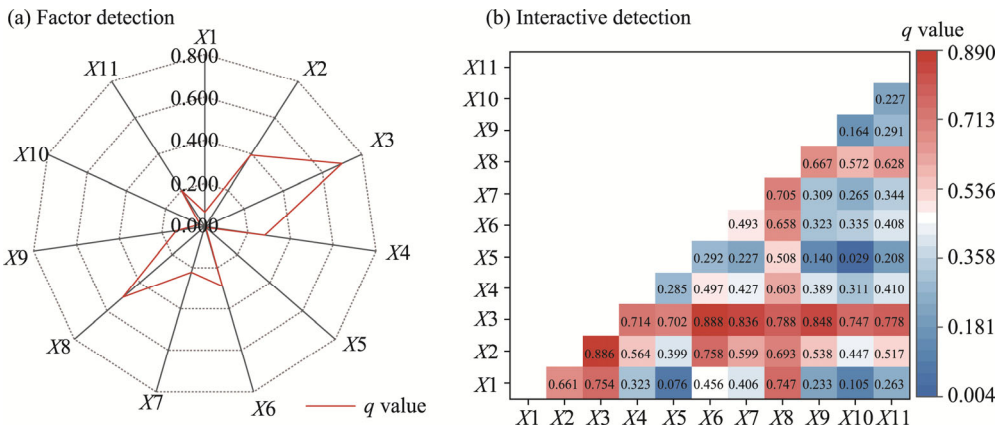

Fig. 7 Factor detection and interactive detection results (indicated by the q values) for various driving factors influencing the spatial differentiation of LST in Xinjiang. (a), factor detection; (b), interaction detection. X_1–X_{11} represent longitude, latitude, DEM, slope, aspect, precipitation, sunshine duration, wind speed, normalized difference vegetation index (NDVI), population density, and land use and land cover (LULC), respectively.

the faster the decrease in surface temperature. If the wind speed is low, the decreases in surface heat will be weakened or disappear, and the surface temperature will increase significantly. When the wind speed increases, the intensity of turbulent mixing increases, and the mixing of high and low temperatures of air results in a more uniform spatial distribution of LST (Ampatzidis and Kershaw, 2020). The influence of latitude on LST showed that the higher the latitude, the smaller the solar elevation angle, the longer the path of solar radiation through the atmosphere, and the greater the weakening and dispersion of light and heat.

In addition, the effects of precipitation, slope, and sunshine duration on the distribution of LST were prominent, with q values of 0.288, 0.280, and 0.221, respectively. Precipitation affects the LST through evaporative cooling, heat transfer, and groundwater recharge (Xi et al., 2023). Precipitation is usually accompanied by the formation of clouds that block direct solar radiation, and reduce surface solar energy input and surface temperature. Slope is the core factor that describes the microtopography, which affects the LST by controlling the local scale of solar radiation and the angle of the prevailing wind direction; the higher the latitude, the greater the influence of microtopographic factors on solar radiation (Zeng et al., 2005). Sunshine duration directly affects the reception time of solar radiation and is an important factor for LST. The more sunshine the ground receives, the greater the solar radiation, the faster the increase in ground temperature, and the higher the LST. The q value of LULC was 0.199, and its influence was second only to that of natural factors. This is because the spatial distribution of LULC is related to the spatial patterns of cold and hot environments on the surface (Wei et al., 2021). Although there are areas of human-dominated change

in the economic belt on the northern slopes of the Tianshan Mountains and in some cities of southern Xinjiang, the Gobi desert area is too large, and the impact of human activities on LST is limited.

The results of interaction detection showed that the explanatory power of a combination of driving factors was stronger than that of a single factor, and the spatial heterogeneity of LST in Xinjiang was enhanced with types of two-factor enhancement or nonlinear enhancement between factors (Fig. 7b). The interaction between DEM and other factors was the most prominent, and the *q* value was greater than 0.700, which further highlights the strong influence of DEM on LST. The interactions of DEM with precipitation (with *q* value of 0.888), latitude (0.885), sunshine duration (0.836), and NDVI (0.848) had the strongest power to explain the spatial heterogeneity of LST, indicating that the spatial differences in precipitation, latitude, and underlying surface vegetation coverage were the main reasons for the enhanced spatial differentiation of LST in the two locations at the same DEM in Xinjiang. The explanatory power of the interaction between wind speed and other factors on LST spatial differentiation was second to that of DEM. The interaction of wind speed with other factors had the second highest explanatory power for the spatial divergence of LST than DEM, and its two-way interaction with aspect had the lowest explanatory power for LST spatial divergence (q=0.508). In single-factor detection, the *q* values of slope and population density were 0.005 and 0.024, respectively, which were significantly enhanced after their interactions with DEM and wind speed. Aspect affects the reception of solar radiation at different DEM and heat distributions. The change rate of LST on the southern slopes of the Tianshan Mountains was lower than that on the northern slopes because the former received more solar radiation. Simultaneously, slope affected the wind speed distribution. When the airflow flows through the slope, the blocking of the terrain accelerates or decelerates the airflow. Xinjiang is sparsely populated, and human activities are concentrated in the plain oasis areas and inland river basins at low DEM. Frequent and high-intensity human activities directly affect surface materials and energy exchange in areas where populations gather. Therefore, LST changes were mainly affected by DEM and human activities in these areas. At the same time, the continuous urban expansion and industrial energy consumption due to human activities have led to changes in construction land, such as the transformation of farmland, natural vegetation, and water bodies into impervious surfaces such as asphalt, concrete, and buildings, which continuously release a large amount of heat. The generated waste heat and smoke also strengthen the atmospheric insulation and inversion effects (Qiao et al., 2019). All of these will directly or indirectly affect the surrounding heat budget balance and increase the heat island effect, and in turn influence the convective and turbulence intensity of local air in the city (Grimmond and Oke, 1999), which can enhance the interaction intensity between population density and wind speed and affect LST.

3.3.2 Attribution analysis using the GWR model

The spatial differentiation of LST in each geomorphic zone was significant. The mountain-scale elevation of the Pakakuna Mountain Group was greater than that of the other mountainous areas, but the correlation between LST and DEM was the weakest. In the middle latitudes of the Tianshan Mountains, the average annual LST was higher than that in the lower latitudes of the Pakakuna Mountain Group, and the average annual LST in the middle latitudes of the Tuha Basin was higher than that in the lower latitudes of the Tarim Basin (Fig. 5). In contrast, the interior of the Tianshan Mountains exhibited a low LST at the same latitude. Although topography had a profound impact on the distribution of LST, it cannot fully explain the spatial heterogeneity of LST and whether there are also spatially heterogeneous correlations with the remaining factors. To answer these questions, this study selected driving factors such as DEM, wind speed, latitude, precipitation, NDVI, and sunshine duration, which provide more powerful explanations for the spatial heterogeneity of LST in the study area, according to the results from the Geodetector model. The GWR model was introduced to identify spatial differences in the direction and intensity of the main driving factors (Fig. 8).

The regression coefficients from the GWR model indicated that each driving factor was spatially non-stationary and showed variability in their characteristics (Table 7). The negative feedback effect

of DEM on the spatial differentiation of LST played a dominant role in the entire Xinjiang and the geomorphological zones; the negative feedback effect was strongest in the Altay Mountains, Junggar Basin, and Tuha Basin. Latitude had a negative feedback effect on the spatial differentiation of LST

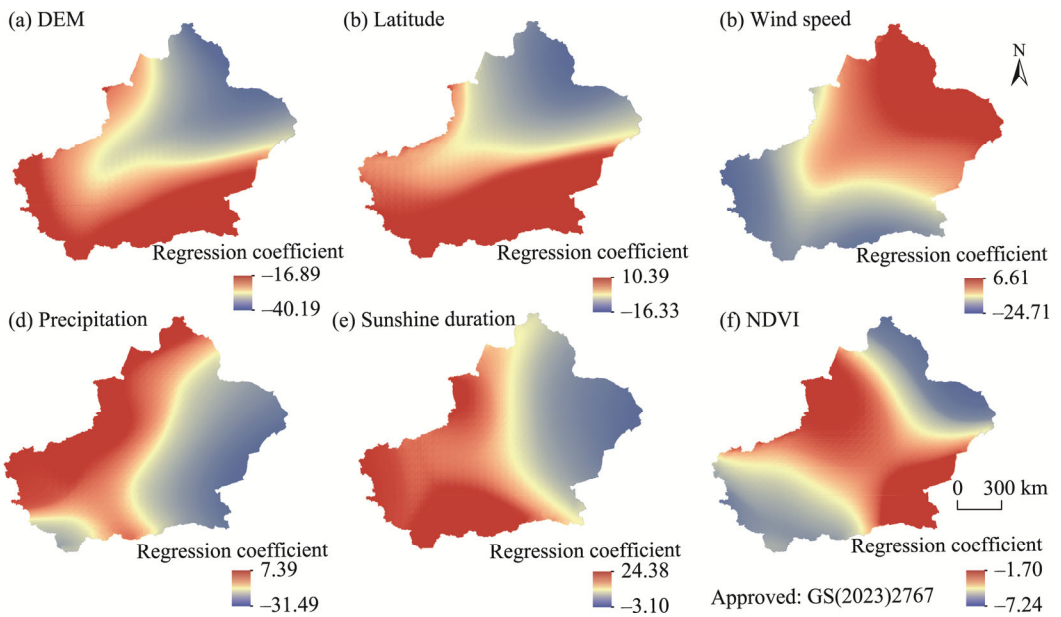

Fig. 8 Spatial distribution of regression coefficients of dominant factors driving the spatial heterogeneity of LST. (a), DEM; (b), latitude; (c), wind speed; (d), precipitation; (e), sunshine duration; (f), NDVI. Note that the figures are based on the standard map (GS(2023)2767) of the Map Service System (https://bzdt.ch.mnr.gov.cn/), and the standard map has not been modified.

Table 7 Regression coefficients of major driving factors in Xinjiang and each geomorphic zone

Geomorphic zone	DEM	Latitude	Wind speed	Sunshine duration	Precipitation	NDVI
Xinjiang	–29.79	–4.71	–8.68	7.18	–7.74	–5.48
Altay Mountains	–38.88	–15.07	2.37	3.89	–2.80	–6.84
Junggar Basin	–35.55	–13.62	0.06	3.95	–5.92	–5.77
Tianshan Mountains	–31.95	–7.75	–6.38	6.43	–5.89	–5.14
Tuha Basin	–35.98	–9.98	2.60	–0.39	–16.56	–6.04
Tarim Basin	–29.56	–3.07	–11.22	8.28	–5.61	–5.39
Pakakuna Mountain Group	–23.05	2.95	–17.43	11.71	–9.10	5.50

in the study area. Each geomorphological zone followed the change rule: the higher the latitude, the stronger the negative feedback effect. The Pakakuna Mountain Group absorbs more solar radiation because of its low latitude; therefore, latitude plays a positive role in the LST differentiation of this geomorphological zone. Precipitation and NDVI had significant negative effects on the LST differentiation. The interaction strength of precipitation and NDVI in each geomorphic unit differed, and the negative effect on the LST differentiation in the Tuha Basin was the most prominent. The annual precipitation and mean NDVI in the Tuha Basin were 2.3 mm and 0.06, respectively, and the aridity, less precipitation, and low vegetation coverage of the neighboring deserts contributed to the increase in LST.

Overall, wind speed negatively affected LST in the study area, and the intensity was second only to the DEM. The wind speed in the Tarim Basin and Pakakuna Mountain Group had a prominent cooling effect on LST, whereas wind speed in the Tuha Basin and Junggar Basin had a weak positive correlation with LST. The interior of the basin is typically surrounded by mountains, forming a

relatively closed terrain. The inversion of cold air in the Tarim Basin and the formation of through-valley rapids owing to the narrow tube effect of topography increased the near-surface wind speed in the Tarim Basin bordering on the Pamir Plateau and Tianshan Mountains, and the rapid flow of air carried away heat from the surface, resulting in lower LST. However, inside the Tuha Basin, owing to the closure of the terrain, the higher the wind speed, the stronger the airflow, and this increased heat removal. Because the mountains provide blocking, it is difficult for heat to be transmitted to the atmosphere through convection and radiation, resulting in a higher LST (Bogren and Gustavsson, 1991; de Wekker et al., 1998). Furthermore, the southeast-down northwest airflow enters the Tuha Basin in a dry and hot environment after turning, and the dry high-temperature wind brought by the increase in wind speed will also increase the LST (Hu, 2004). Simultaneously, some studies have indicated that the spatial distribution relationship between LST and wind speed is related to the season, and wind speed is positively correlated with LST in summer (e.g., Yu, 2017).

Among all driving factors, only the influence of sunshine duration on LST was positive, and only the LST change in the Tuha Basin was weakly negatively correlated with sunshine duration. The lower latitudes of the Pakakuna Mountain Group and Tarim Basin are geomorphic zones that receive the longest duration of solar radiation in all geomorphic zones; sunshine duration has the strongest positive feedback effect. The annual average LST of the Tarim Basin was lower than that of the Tuha Basin, which was partly due to the low level of the terrain in the Tuha Basin (140–1117 m), and the cooling effects of precipitation and NDVI were less than those in the Tuha Basin. However, it was also due to the negative feedback effect and cooling effect of wind speed in the Tarim Basin, which was second only to that of the Pakakuna Mountain Group. Although sunshine duration had a negative feedback effect on the LST of the Tuha Basin, its influence was far less than that of the other factors, which weakened the control intensity of latitudinal zonality on the LST of the Tuha Basin.

In general, DEM was the main factor determining the spatial differentiation of LST in Xinjiang. Low latitude, low vegetation coverage, less precipitation, and long sunshine duration were conducive to warming; however, not all geomorphological zones followed this trend. Periodic and local differences existed in the spatial heterogeneity of LST caused by wind speed. The spatial heterogeneity of the regional LST was formed by the combined influence of various driving factors. Whether there is spatial differentiation in the seasonal LST in geomorphological zones requires further investigation.

3.4 Source-sink effect on LST in Xinjiang

Spatial distribution of LST and thermal environmental characteristics in the study area were primarily due to the combined effect of small regional topography and underlying surface properties. LULC has different physical properties, such as reflectivity, roughness, and humidity, which can affect the change in energy and material exchange between the ground and atmosphere, thereby altering the climate (Chi et al., 2021). The concept of source-sink is an important ecological process/pattern concept (Wu et al., 2022). Promoting the generation of geographical phenomena is called a source, while inhibiting the development of geographical phenomena is called a sink. The energy cycle between the two can reflect the differences in ecological processes to a certain extent (Wu et al., 2022). The heterogeneity of the underlying surfaces in the arid areas is strong, and there are numerous manufacturing changes in the LULC (Mao et al., 2017). To a certain extent, it can also reflect the influence of human activities on LST distribution. In natural ecology, land cover can better reflect the influence of vegetation on LST (Chen et al., 2022a). Therefore, the introduction of the source-sink theory to explore the heat source and heat sink effects of different LULC types in the surface thermal environment can provide a reference for alleviating urban heat islands, protecting and planning ecosystems, and restoring vegetation and water bodies to promote sustainable development in arid areas.

This study calculated the source-sink effect identification results for different LULC types based on LST in the study area from 2000 to 2020 (Fig. 9a and b). Owing to the complexity of the LULC types and the large uncertainty in the LST changes of the converted LULC types with a small area of each geomorphic zone, only a detailed analysis of the source-sink effect of LULC in each geomorphic zone in 2020 was conducted (Table 8). Simultaneously, the CI values of different LULC

types to the LST were also calculated. A positive CI value indicates the warming amount per square kilometer, and vice versa (Fig. 9c). The results showed that unused land was the most stable heat source in Xinjiang and the source-sink effects and contribution indices of different LULC types in different geomorphological zones differed.

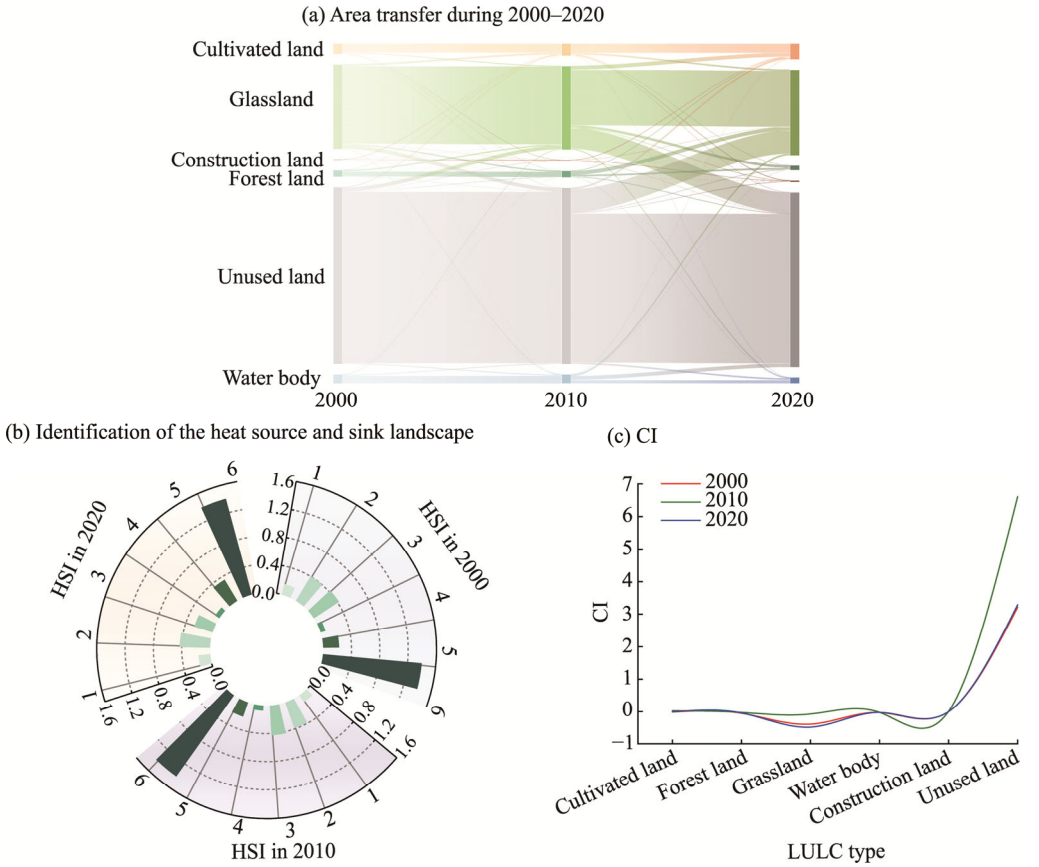

Fig. 9 Area transfer among different LULC types (a), identification of the heat source and sink landscape (HSI; b), and contribution index (CI) of each LULC type to LST (c) in Xinjiang during 2000–2020. In Figure 9b, each color of the bar chart corresponds to each LULC type; numbers of 1–6 represent cultivated land, forest land, grassland, water body, construction land, and unused land, respectively.

Table 8 Identification of the heat source and sink landscape (HSI) and contribution index (CI) of each LULC type to LST in Xinjiang and each geomorphic zone in 2020

Geomorphic zone	Cultivated land		Forest land		Grassland		Water body		Construction land		Unused land	
	HSI	CI	HSI	CI	HSI	CI	HSI	CI	HSI	CI	HSI	CI
Xinjiang	0.17	–0.0105	0.43	–0.0429	0.27	–0.4827	0.07	–0.0272	0.35	–0.0002	1.40	3.2874
Altay Mountains	2.19	0.0761	0.27	–0.2588	1.20	0.7801	0.29	–0.0667	2.68	0.0198	0.66	–0.5347
Junggar Basin	0.08	–0.2278	0.00	–0.0015	1.13	–0.0534	0.69	–0.0011	2.84	0.0097	1.03	0.2742
Tianshan Mountains	0.94	0.1109	0.07	–0.1475	0.49	–0.9431	0.23	–0.2640	1.24	0.0181	1.88	1.2357
Tuha Basin	0.86	–0.0031	3.92	0.0002	2.95	0.0124	0.00	–0.0001	1.07	–0.0013	0.98	0.0083
Tarim Basin	0.01	–0.2255	0.03	–0.1114	0.47	–0.1933	0.02	–0.0263	0.04	–0.0074	1.12	0.5638
Pakakuna Mountain Group	3.42	0.0241	2.19	0.0025	1.11	0.0819	0.15	–0.6998	3.40	0.0023	1.00	0.5928

Only unused land (with HSI>1.00) had a source effect on the LST changes in Xinjiang during 2000–2020. In contrast, cultivated land, forest land, grassland, water body, and construction land (with HSI<1.00) had sink effects on the LST changes. Unused land accounted for an average of

61.02% of the total area in Xinjiang during 2000–2020. These areas are usually without human activities or vegetation coverage, and their bare surfaces have a low level of reflectivity and can absorb more solar radiation and convert it into heat (Qu et al., 2014). These areas are the main geothermal resource producers in Xinjiang. In 2010, 20,443 and 45,663 km^2 of grassland and water body were converted to unused land, respectively, resulting in a warming of 6.61°C/km^2 in unused land in 2010; 153,200 km^2 of unused land was converted to grassland, cultivated land, and other LULC types that showed typical heat-sink effects in the period from 2010 to 2020, which resulted in the warming produced by the unused land decreasing to 3.29°C/km^2. The area proportion of unused land in the Tarim Basin in 2020 was as high as 84.95%, and this was the main heat source of LST in the geomorphic zone, with a LST increase of 0.56°C/km^2. Although the area of the unused land in the Tianshan Mountains was small, it had a prominent source effect, with a LST increase of 1.24°C/km^2 in unused land. The HSI value of water body was the smallest, and its heat sink effect was the most prominent as a dominant type of cooling. However, the water body only decreased the LST by 0.02°C/km^2, while the heat sink effect of water body was decreasing due to a reduction in area. The maximum cooling effect of water body was 0.70°C/km^2 in the Pakakuna Mountain Group. The surfaces of forest land and grassland with high vegetation coverage can absorb part of solar radiation, and transpiration can consume a large amount of heat. Simultaneously, vegetation has a high specific heat capacity and heat conduction ability and can store and release large amounts of heat. Forest land and grassland provide a certain degree of shade, which can reduce the input of surface heat (Bonan, 2008). As the area of water body in Xinjiang is much smaller than those of grassland and forest land, the cooling effect is weaker. Therefore, grassland and forest land were the most prominent LULC types with a heat sink effect in Xinjiang. In 2020, the LST was reduced by 0.48°C/km^2 in grassland. Grassland and forest land in some geomorphic zones showed a heat source effect. For example, the Altay Mountains, Tuha Basin, and Pakakuna Mountain Group with low vegetation coverage showed a heat source effect, and the remaining geomorphic zones exhibited the heat sink effect. The cooling effects of forest land and grassland in the Tianshan Mountains were the highest, decreasing the LST at 0.15°C/km^2 and 0.94°C/km^2, respectively. In arid areas, vegetation is usually a heat source rather than a heat sink during the non-growing period (Li et al., 2004). A dry environment leads to higher soil thermal conductivity, which facilitates heat conduction. During the non-growth period, vegetation absorbs and stores a large amount of heat, converts solar radiation into heat during the day, and releases the stored heat at night, resulting in a relatively high LST. In 2020, 28.99% of the increase in construction land came from unused land. The increase in impervious surface area caused by the conversion of cultivated land and grassland into construction land can enhance the heat island effect (Dong, 2012; Zeng, 2015). In contrast, the conversion of large areas of unused land, such as deserts and bare land, to construction land results in cooling. Although the same is true for the expansion of construction land, the transformation of different LULC types by human activities has different positive and negative effects. With the development of social economy, human activities such as land reclamation and agricultural planting have led to the expansion of cultivated land and increased the related heat sink effects. The heat sink effect of cultivated land is primarily related to agricultural irrigation area and crop growth status, and the heat sink effect of cultivated land in the Junggar Basin was the most prominent. Studies have shown that water-saving irrigation can improve water-use efficiency and increase the net heat sink (Zhang et al., 2022). The heat sink effect of cultivated land may also impact climate and ecosystems, thereby affecting temperature distribution and precipitation patterns. It may also affect biodiversity, soil moisture, and crop growth. Therefore, in agricultural planning and land-use management, it is necessary to consider and make rational use of the heat sink effect of cultivated land.

In summary, the source-sink effects of LULC in Xinjiang had a particular regulatory impact on LST. Owing to the influences of vegetation types, soil types, climatic conditions, and human activities, there are significant differences of LST in each geomorphic zone. Unused land is the most common LULC type in Xinjiang, and makes the largest contribution to the increase in LST. A reasonable transformation of human activities can moderately reduce the heat source effect of unused land. Water body was the most important heat sink landscape, greatly affecting the water ecosystem and biodiversity. Although melting glacier snow as a heat sink is conducive to the water conservation function of mountains and water security downstream, in the long run, further reduction of glacier

snow is not conducive to the ecosystem balance. The heat sink effect on land is primarily produced by crop vegetation; however, the heat sink effect of some vegetation in arid areas is related to the growth period. Grassland and forest land are the most prominent land cover types associated with the heat sink effect. In addition to the strict control of forest cutting, it is necessary to strictly prohibit the reclamation of shrubland and grassland and attach importance to the function and value of desert biodiversity, which is more valuable than extensive and backward utilization methods, such as reclamation and grazing. The degree to which cultivated land is considered a heat source or heat sink is affected by many natural factors, management methods, and agricultural activities. For example, improving the utilization efficiency of water resources in arid areas can effectively enhance the heat sink effect of cultivated land, maintain the temperature of soil and vegetation in winter, and prevent freezing and disasters. However, excessive heat sink effects can lead to soil drought and water evaporation. Therefore, to manage cultivated land and agricultural production, it is necessary to comprehensively consider and balance various factors to maximize the positive role of the heat source and heat sink effects and reduce their negative impacts. In addition, the impact of human activities on the ground temperature cannot be ignored. When the anthropogenic destruction of vegetation leads to an increase in secondary unused land, the degradation of vegetation and conversion of forest land to grassland or bare land with low vegetation coverage can lead to regional warming. Therefore, understanding and studying the impacts of these factors on the source-sink effect will aid in rational planning and management, reduce adverse effects on the environment and ecosystems, and ensure regional ecological security.

4 Conclusions

This study analyzed the spatial and temporal differentiation patterns of LST in Xinjiang from 2000 to 2020. The Geodetector and GWR models were used to determine the mechanisms driving the spatial differentiation of LST at different scales. The main conclusions are as follows:

(1) During the study period, the multi-year average LST in Xinjiang was 9.45°C, which showed an overall warming trend (0.24°C/10a) with vast warming area. The Tuha Basin and Tarim Basin are the most stable geomorphologic zones in terms of warming. Mountainous areas were identified as the primary cooling zones, but several significant warming zones in the western part of the Tianshan Mountains were also identified. DEM was found to play a prominent role in LST changes. The LST was characterized by latitudinal zonation under the influence of solar radiation, and the underlying surface strengthened its spatial heterogeneity by influencing local surface thermal properties.

(2) There were significant seasonal variations in LST in the study area. Among the four seasons, only autumn was identified as cooling at a rate of 0.09°C/10a. The other seasons all showed a warming trend, with the fast warming rate in spring (0.49°C/10a), followed by winter (0.48°C/10a). Seasonal variability in all geomorphic zones was consistent with that of LST in Xinjiang except for the Pakakuna Mountain Group, which, to a certain extent, reflected their climatic sensitivity and indicativeness.

(3) The spatial distribution of LST in Xinjiang was dominated by topographic and locational factors, followed by natural factors. DEM, wind speed, and latitude also contributed significantly. The interactions among factors had a greater effect on the spatial differentiation of LST than a single factor. The strength of the interactions between DEM and other driving factors was the greatest. Specifically, the interactions of DEM with precipitation (q value of 0.888), latitude (0.885), and NDVI (0.848) can better explain the spatial heterogeneity of LST, emphasizing the strong influence of DEM.

(4) There was obvious spatial heterogeneity in the direction and strength of the effects of the driving factors on the spatial differentiation of LST in Xinjiang. Only sunshine duration was positively correlated with the spatial differentiation in LST, and the negative feedback effect of DEM was the strongest. Low latitude, low vegetation coverage, less precipitation, and long sunshine duration favored an increase in LST. The driving factors for each geomorphological zone were subject to the atmospheric circulation at different spatial and temporal scales, and there were cyclic and local differences in the process coupled with the formation of a unique local circulation system, resulting in seasonal variations in the driving mechanisms.

(5) The source-sink effects of LULC types in Xinjiang had regulatory effects on LST, and there were significant differences in their influences in various geomorphologic zones due to their vegetation types, climatic conditions, soil types, human activities, and other factors. Unused land was the most common LULC type in Xinjiang and contributed the most to increases in LST, whereas water body was the most important heat sink, and the heat sink effect on land was primarily generated by crop vegetation. Grassland and forest land were the main LULC types with the most prominent heat sink effects, but these were related to the growth period in arid zones.

Analysis of the spatiotemporal evolution of LST in Xinjiang and its driving mechanisms helps to quantitatively determine the factors driving the spatial heterogeneity of LST in Xinjiang and investigate their spatial relationship. The source-sink effects of different LULC types on LST in Xinjiang were also explored to provide a reference for understanding climate change and planning sustainable development of oases in arid regions. Based on an attribution analysis of the spatial differentiation of LST at the inter-annual scale, the changes in LST were found to be affected by numerous factors and some geomorphological zones had unique mechanisms of action. Therefore, it is necessary to consider whether there are differences in the response mechanism of LST at different time scales. Furthermore, in geographical studies, the results are affected by the size of the analysis unit. Due to the sparse vegetation and small population in Xinjiang, human activities are relatively weak, if the scale is too large, the study may not reflect the impacts of human factors on LST. In future research, analysis of the spatial distribution characteristics and causes of LST based on multiple time scales (such as seasonal, monthly, and daily) should be conducted. Attempts can be made to analyze the relationship between LST and natural and socioeconomic factors based on study units with different underlying surfaces and grain sizes.

Conflict of interest

The authors declare that they have no known competing financial interests or personal relationships that could have appeared to influence the work reported in this paper.

Acknowledgements

This research was supported by the Third Xinjiang Scientific Expedition Program (2021xjkk0801).

Author contributions

Conceptualization: ZHANG Mingyu, ZHANG Zhengyong; Methodology: ZHANG Mingyu, ZHANG Zhengyong, CAO Yu, ZHANG Xueying; Formal analysis: ZHANG Mingyu, ZHANG Zhengyong, CAO Yu, LIU Lin; Writing - original draft preparation: ZHANG Mingyu, ZHANG Zhengyong; Writing - review and editing: ZHANG Mingyu, ZHANG Zhengyong, CAO Yu, ZHANG Xueying; Funding acquisition: ZHANG Zhengyong; Resources: CHEN Hongjin, YU Fengchen; Supervision: GAO Yu, YU Fengchen, LIU Xinyi. All authors approved the manuscript.

References

Ampatzidis P, Kershaw T. 2020. A review of the impact of blue space on the urban microclimate. Science of the Total Environment, 730: 139068, doi: 10.1016/j.scitotenv.2020.139068.

Anderson M C, Norman J M, Kustas W P, et al. 2008. A thermal-based remote sensing technique for routine mapping of land-surface carbon, water and energy fluxes from field to regional scales. Remote Sensing of Environment, 112(12): 4227–4241.

Bogren J, Gustavsson, T. 1991. Nocturnal air and road surface temperature variations in complex terrain. International Journal of Climatology, 11(4): 443–455.

Bonan G B. 2008. Forests and climate change: Forcings, feedbacks, and the climate benefits of forests. Science, 320(5882): 1444–1449.

Brenning A, Peña M A, Long S, et al. 2012. Thermal remote sensing of ice-debris landforms using ASTER: An example from the Chilean Andes. The Cryosphere, 6(2): 367–382.

Brunsdon C, Fotheringham A S, Charlton M E. 1996. Geographically weighted regression: A method for exploring spatial nonstationarity. Geographical Analysis, 28(4): 281–298.

Chen H J, Liu L, Zhang Z Y, et al. 2022a. Spatio-temporal correlation between human activity intensity and land surface temperature on the north slope of Tianshan Mountains. Journal of Geographical Sciences, 32(10): 1935–1955.

Chen Y, Baishan J, Shao W, et al. 2022b. Influence of Arctic Oscillation on winter temperature in Xinjiang under climate warming background. Journal of Arid Meteorology, 40(2): 195–201. (in Chinese)

Chi Q, Zhou S H, Wang L J, et al. 2021. Quantifying the contribution of LUCC to surface energy budget: A case study of four typical cities in the Yellow River Basin in China. Atmosphere, 12(11): 1374, doi: 10.3390/atmos12111374.

De Wekker S F J, Zhong S Y, Fast J D, et al. 1998. A numerical study of the thermally driven plain-to-basin wind over idealized basin topographies. Journal of Applied Meteorology and Climatology, 37(6): 606–622.

Dong D W, Tao H, Ding G, et al. 2022. Historical population and cropland exposure to heatwaves in Xinjiang, China. Transactions of the Chinese Society of Agricultural Engineering, 38(5): 288–295. (in Chinese)

Dong L P. 2012. Estimation of surface air temperature from MODIS land surface temperature and its application to the study of urban heat island in the East China Metropolitan Area. MSc Thesis. Nanjing: Nanjing University of Information Science and Technology. (in Chinese)

Fu Q, Li B, Hou Y, et al. 2017. Effects of land use and climate change on ecosystem services in Central Asia's arid regions: A case study in Altay Prefecture, China. Science of the Total Environment, 607–608: 633–646.

Garratt J R. 1994. Review: The atmospheric boundary layer. Earth-Science Reviews, 37(1–2): 89–134.

Grimmond C S B, Oke T R. 1999. Aerodynamic properties of urban areas derived from analysis of surface form. Journal of Applied Meteorology and Climatology, 38(9): 1262–1292.

Hachem S, Duguay C R, Allard M. 2012. Comparison of MODIS-derived land surface temperatures with ground surface and air temperature measurements in continuous permafrost terrain. The Cryosphere, 6(1): 51–69.

Han J, Rui Y, Yang K, et al. 2020. Quantitative attribution of national key town layout based on Geodetector and the geographically weighted regression model. Progress in Geography, 39(10): 1687–1697. (in Chinese)

Hu R J. 2004. Physical Geography of the Tianshan Mountains in China (2nd ed.). Beijing: China Environmental Science Press, 70–77. (in Chinese)

Hu T, van Dijk A I J M, Renzullo L J, et al. 2020. On agricultural drought monitoring in Australia using Himawari-8 geostationary thermal infrared observations. International Journal of Applied Earth Observation and Geoinformation, 91: 102153, doi: 10.1016/j.jag.2020.102153.

Huang F F, Ma W Q, Li M S, et al. 2016. Analysis on responses of land surface temperature on the northern Tibetan Plateau to climate change. Plateau Meteorology, 35(1): 55–63. (in Chinese)

Kang Z W, Zhang Z Z, Liu L, et al. 2022. Spatio-temporal variation characteristics of land surface temperature in Xinjiang based on MODIS. Geographical Research, 41(4):997–1017. (in Chinese)

Khan J, Wang P X, Xie Y, et al. 2018. Mapping MODIS LST NDVI imagery for drought monitoring in Punjab Pakistan. IEEE Access, 6: 19898–19911.

Li K R, Wang S Q, Cao M K. 2004. Vegetation and soil carbon storage in China. Science in China Series D-Earth Sciences, 47(1): 49–57.

Li Q X, Sun W B, Huang B Y, et al. 2020. Consistency of global warming trends strengthened since 1880s. Science Bulletin, 65(20): 1709–1712.

Li Z L, Tang B H, Wu H, et al. 2013. Satellite-derived land surface temperature: Current status and perspectives. Remote Sensing of Environment, 131: 14–37.

Liu L, Liu P X, Zhang W X, et al. 2021. Variation characteristics of extreme warm events from 1961 to 2017 and projection for future scenarios in Xinjiang, China. Arid Zone Research, 38(6): 1590–1600. (in Chinese)

Mao D L, Cai F Y, Lei J Q, et al. 2017. Spatial analysis on changes of microclimate in typical landscapes in desert-wilderness-oasis in Cele, Xinjiang. Scientia Geographica Sinica, 37(4): 630–640. (in Chinese)

Ning S, Zhang Z Y, Liu L, et al. 2020. Adaptability of precipitation estimation method based on TRMM data combined with partial least squares downscaling in different landforms of Xinjiang, China. Transactions of the Chinese Society of Agricultural Engineering, 36(12): 99–109. (in Chinese)

Pan N H, Guan Q Y, Wang Q Z, et al. 2021. Spatial differentiation and driving mechanisms in ecosystem service value of arid region：A case study in the middle and lower reaches of Shule River Basin, NW China. Journal of Cleaner Production, 319: 128718, doi: 10.1016/j.jclepro.2021.128718.

Portela C I, Massi K G, Rodrigues T, et al. 2020. Impact of urban and industrial features on land surface temperature: Evidences

from satellite thermal indices. Sustainable Cities and Society, 56: 102100, doi: 10.1016/j.scs.2020.102100.
Qiao Z, Huang N Y, Xu X L, et al. 2019. Spatio-temporal pattern and evolution of the urban thermal landscape in metropolitan Beijing between 2003 and 2017. Acta Geographica Sinica, 74(3): 475–489. (in Chinese)
Qu Y, Liu Q, Liang S L, et al. 2014. Direct-estimation algorithm for mapping daily land-surface broadband albedo from MODIS data. IEEE Transactions on Geoscience and Remote Sensing, 52(2): 907–919.
Ren T, Zhou W Q, Wang J. 2021. Beyond intensity of urban heat island effect: A continental scale analysis on land surface temperature in major Chinese cities. Science of the Total Environment, 791: 148334, doi: 10.1016/j.scitotenv.2021.148334.
Sfîcă L, Corocăescu A C, Crețu C Ș, et al. 2023. Spatiotemporal features of the surface urban heat island of Bacau City (Romania) during the warm season and local trends of LST imposed by land use changes during the last 20 years. Remote Sensing, 15(13): 3385, doi: 10.3390/rs15133385.
Shi Y F, Cheng G D. 1991. Cryosphere and global change. Bulletin of Chinese Academy of Sciences, (4): 287–291. (in Chinese)
Tian H, Liu L, Zhang Z Y, et al. 2022. Spatiotemporal diversity of land surface temperature in China from 2001 to 2020. Acta Geographica Sinica, 77(7):1713–1729. (in Chinese)
Townshend J R G, Justice C O, Skole D, et al. 1994. The 1 km resolution global data set: Needs of the International Geosphere Biosphere Programme. International Journal of Remote Sensing, 1994, 15(17): 3417–3441.
Wan G N, Yang M X, Wang X J. 2012. Variations in soil temperature at BJ site on the central Tibetan Plateau. Journal of Mountain Science, 9(2): 274–285.
Wang J F, Xu C D. 2017. Geodetector: Principle and prospective. Acta Geographica Sinica, 72(1): 116–134. (in Chinese)
Wang L L, Gao Z Q, Miao S G, et al. 2015. Contrasting characteristics of the surface energy balance between the urban and rural areas of Beijing. Advances in Atmospheric Sciences, 32: 505–514.
Wei B C, Bao Y H, Yu S, et al. 2021. Analysis of land surface temperature variation based on MODIS data a case study of the agricultural pastural ecotone of northern China. International Journal of Applied Earth Observation and Geoinformation, 100: 102342, doi: 10.1016/j.jag.2021.102342.
Wu J S, He H S, Hu T. 2022. Analysis of factors influencing the "source-sink" landscape contribution of land surface temperature. Acta Geographica Sinica, 77(1): 51–65. (in Chinese)
Xi M Z, Zhang W, Li W L, et al. 2023. Distinguishing dominant drivers on LST dynamics in the Qinling-Daba Mountains in Central China from 2000 to 2020. Remote Sensing, 15(4): 878, doi: 10.3390/rs15040878.
Yang Z W, Chen Y B, Guo G H, et al. 2021. Characteristics of land surface temperature clusters: Case study of the central urban area of Guangzhou. Sustainable Cities and Society, 73: 103140, doi: 10.1016/j.scs.2021.103140.
Yu Z. 2017. Changes of ground temperature in Sichuan and evaluation model. PhD Dissertation. Chengdu: Chengdu University of Technology. (in Chinese)
Yu Z W, Chen T T, Yang G Y, et al. 2020. Quantifying seasonal and diurnal contributions of urban landscapes to heat energy dynamics. Applied Energy, 264: 114724, doi: 10.1016/j.apenergy.2020.114724.
Yue S P, Yan Y C, Zhang S W, et al. 2021. Spatiotemporal variations of soil freeze-thaw state in Northeast China based on the ERA5-LAND dataset. Acta Geographica Sinica, 76(11): 2765–2779. (in Chinese)
Zeng J. 2015. Remote sensing monitoring of land use change impacts on land surface temperature. MSc Thesis. Guilin: Guangxi Normal University. (in Chinese)
Zeng L L, Wardlow B D, Tadesse T, et al. 2015. Estimation of daily air temperature based on MODIS land surface temperature products over the Corn Belt in the US. Remote Sensing, 7(1): 951–970.
Zeng Y, Qiu X F, Liu C M, et al. 2005. Distributed modelling of direct solar radiation of rugged terrain over the Yellow River Basin. Acta Geographica Sinica, 60(4): 680–688. (in Chinese)
Zhang F, Tiyip T, Kung H, et al. 2016. Dynamics of land surface temperature (LST) in response to land use and land cover (LULC) changes in the Weigan and Kuqa river oasis, Xinjiang, China. Arabian Journal of Geosciences, 9: 499, doi: 10.1007/s12517-016-2521-8.
Zhang F F, Peng K, Zhang F. 2022. Spatial distribution characteristics of land surface temperature and its "source-sink" effect in Yanqi Basin, Xinjiang. Transactions of the Chinese Society of Agricultural Engineering, 38(16): 153–161. (in Chinese)
Zhang G L, Xiao X M, Dong J W, et al. 2015. Mapping paddy rice planting areas through time series analysis of MODIS land surface temperature and vegetation index data. ISPRS Journal of Photogrammetry and Remote Sensing, 106: 157–171.
Zhang M Y, Zhang Z Y, Liu L, et al. 2023. Spatio-temporal pattern and attribution analysis of mass elevation effect in Tianshan Mountains of China. Acta Geographica Sinica, 78(05): 1254–1270. (in Chinese)
Zhang Q, Xu C Y, Zhang Z X, et al. 2009. Changes of temperature extremes for 1960–2004 in Far-West China. Stochastic Environmental Research and Risk Assessment, 23: 721–735.
Zhang Z Y, Liu L, He X L, et al. 2019. Evaluation on glaciers ecological services value in the Tianshan Mountains, Northwest China. Journal of Geographical Sciences, 29: 101–114.
Zheng K Y, Tan L S, Sun Y W, et al. 2021. Impacts of climate change and anthropogenic activities on vegetation change: Evidence from typical areas in China. Ecological Indicators, 126: 107648, doi: 10.1016/j.ecolind.2021.107648.
Zhou J, Zhang X, Zhan W F, et al. 2014. Land surface temperature retrieval from MODIS data by integrating regression models and the genetic algorithm in an arid region. Remote Sensing, 6(6): 5344–5367.